Atomistic approach to simulate kink migration and kink-pair formation in silicon: The kinetic activation-relaxation technique

Simen N. H. Eliassen,[1] Jesper Friis,[2] Inga G. Ringdalen,[2] Normand Mousseau,[3] Mickaël Trochet,[3,4] and Yanjun Li[1]
[1]*Department of Materials Science and Engineering, Norwegian University of Science and Technology (NTNU), N-7491 Trondheim, Norway*
[2]*SINTEF Industry, Trondheim, Norway*
[3]*Département de physique and Regroupement québécois sur les matériaux de pointe, Université de Montréal, Case postale 6128, succursale center-ville, Montréal (QC), Canada H3C 3J7*
[4]*DEN/DMN-Service de Recherches de Métallurgie Physique, CEA, F-91191 Gif-sur-Yvette, France*

(Received 29 April 2019; revised manuscript received 9 August 2019; published 21 October 2019)

The energy conversion efficiency of solar cells based on multicrystalline silicon is greatly deteriorated by dislocations. However, an in-depth understanding on the dislocation motion dynamics down to atomic scale is still lacking. In this paper, we propose a novel atomistic approach to simulate the kink migration and kink-pair formation which govern dislocation motion in silicon, namely the kinetic activation-relax technique (k-ART). With this method, long timescale events can be simulated and complex energy landscapes can be explored. Four mechanisms for kink migration are observed, with total activation energy of 0.16, 0.25, 0.32, and 0.25 eV. New nontrivial kink structures that participate in kink migration are identified due to the open-ended search algorithm for saddle points in k-ART. In addition, a new pathway for kink-pair formation, with a minimum activation energy of 1.11 eV is discovered. The effect of shear stress on kink migration is also investigated. It shows that shear stress shifts the energy barriers of available events to lower energies, resulting in a change of the preferred kink-migration mechanism and a reduction of kink-pair formation energy.

DOI: 10.1103/PhysRevB.100.155305

I. INTRODUCTION

Single-crystal and multicrystalline silicon (mc-Si) are widely used for solar cell applications. Production of the former results in an almost defect-free crystalline material at the expense of low productivity and high energy consumption, whilst the latter exhibit various crystalline defects and impurities with lower production costs and higher potential for large production scale. The presence of defects in mc-Si greatly reduces the overall conversion efficiency and there are still a large room for improvements [1,2]. Dislocations, in particular, are proven to be especially detrimental to the lifetime of minority charge carriers [3,4]. However, atomistic details of the dislocation dynamics are still lacking, and an in-depth understanding on the underlying mechanisms responsible for the nucleation and migration of dislocations can potentially lead to better material quality and subsequently increase the conversion efficiency of silicon solar cells.

Silicon crystals have a diamond structure with two sets of {111} planes: the narrowly spaced plane (glide set) and the widely spaced plane (shuffle set). At high temperature and low stress, dislocations are either screw dislocations or 60° dislocations, the former of which dissociates into two 30° Shockley partials, while the latter into 30° and 90° Shockley partials [5]. Large experimental efforts have been devoted to characterize the dislocations in this regime [6–8], and the common conclusion is that they are positioned in the narrowly spaced glide set, and slip in the same set. In the low-temperature and high-stress conditions, experimental studies also show that the dislocations prefer their undissociated state [9,10]. Whether the dislocations are located in the glide or shuffle set is not yet firmly established [11,12], but the general consensus is that in the low-temperature and high-stress regime, the dislocations are positioned in the widely spaced shuffle set, and slip in the same set.

In silicon, kink-pair formation and kink migration govern the dislocation motion, and can be described as a sequence of bond breaking and creation. The covalent nature of bonds in silicon leads to a high activation energy for dislocation motion in comparison to metals [5,13]. Theoretical estimations of kink formation energy F_k and kink migration energy W_k have been done for the partial dislocations [14–21], while there only exist a few studies on the undissociated dislocation [22,23]. Despite numerous simulation studies, results are not conclusive due to the large scatter of calculated energies, possibly related to the myriad existence of kink configurations [24].

Dislocation motion in silicon is considered as a rare event due to the steep Peierls valleys; thus, the timescale limitation of conventional molecular dynamics makes this method not well-suited to simulate such mechanisms. Therefore most calculations of the kink-pair formation energy and kink migration energy have been based on the nudged elastic band (NEB) method [25,25] in combination with either density functional theory (DFT) or interatomic potentials. NEB simulation require knowledge of the initial and final states, and an initial guess for the connecting pathway. This means that only the pathway closest to the initial guess is explored, leaving other possible pathways unexplored. This can be problematic with complex energy landscapes, where nontrivial but relevant pathways may be present.

 ©2019 American Physical Society

Core structure of kinks on dislocations and their role in dislocation motion in silicon have been considered to be of high complexity [26]. To thoroughly sample the energy landscape around such complex structures and reveal new possible nontrivial structures, an open-ended search algorithm is a necessity. In principle, such a method can perform an unbiased exploration of the energy landscape, and potentially find all possible transitions from the initial configuration. Together with a kinetic Monte Carlo (KMC) scheme, nonintuitive kink structures and new energy pathways may present themselves as the system evolves.

In this study, we present a novel approach to simulate the kink migration and kink-pair formation in silicon. A kinked undissociated screw dislocation placed in the shuffle set is investigated with k-ART, an off-lattice KMC algorithm. A topological approach is utilized to classify local off-lattice configurations present in systems involving dislocations. Transitions are found by an open-ended search for saddle points. Using k-ART, new intermediate kink structures that participate in kink migration were revealed; furthermore, with the comprehensive search for saddle points, a new minimum energy pathway for kink migration and kink-pair formation is presented.

The paper is organized as follows. First, the methodology is described, including a description of k-ART, the model employed and the computational details. The results and discussion section is divided into three parts. In the first part, overall time evolution for all three stress levels are presented. The second part goes into the atomic details of kink migration, whilst the third part concerns the kink-pair formation. In particular, we mainly focus on the atomic details for both mechanisms, identifying which energy pathways are favored for kink migration and kink-pair formation and the associated atomic configurations. The effect of shear stress on the energy barriers is also presented. In the end, key findings in this study are summarized with conclusions and outlook.

II. METHODOLOGY

A. Kinetic activation-relaxation technique

K-ART is an off-lattice kinetic Monte Carlo (KMC) based method with an open-ended search for saddle points and on-the-fly cataloguing. K-ART can be divided into three parts: a topological classification, a searching method for saddle points and, the analysis and selection of the events according to transition state theory. All events that are generated are cataloged on-the-fly as the system evolves and can be reused throughout the simulation. A workflow of the k-ART algorithm is illustrated in Fig. 1 and the general steps are described in the following sections. For more in-depth details of the method, the reader is referred to the following papers [27–30].

1. Topological classification

K-ART classifies the atomic structure through graph theory, which provides the possibilities to categorize complex and off-lattice atomic arrangements while taking into account long- and short-range elastic interactions.

Graphs are constructed by considering a sphere with a predefined radius around each atom in the system as illustrated in Fig. 2. The sphere radius depends on the system under investigation, but is typically selected to be between 5 and 7 Å, a region that counts between 40 and 80 atoms. The atoms within the sphere are connected by considering a neighbor prescription, e.g., first neighbor distance cutoff, which results in a truncated connectivity graph. This graph is then analyzed by NAUTY, a topological analysis library developed by McKay [31]. NAUTY provides a unique automorphic group identifier for each atom with an associated table linking the vertices of a reference graph.

Geometrical information is lost during the topological classification. However, a complete reconstruction from a topological graph is possible since we know the positions of all atoms surrounding the local graph, which allows the algorithm to reconstruct a unique and fully relaxed geometry

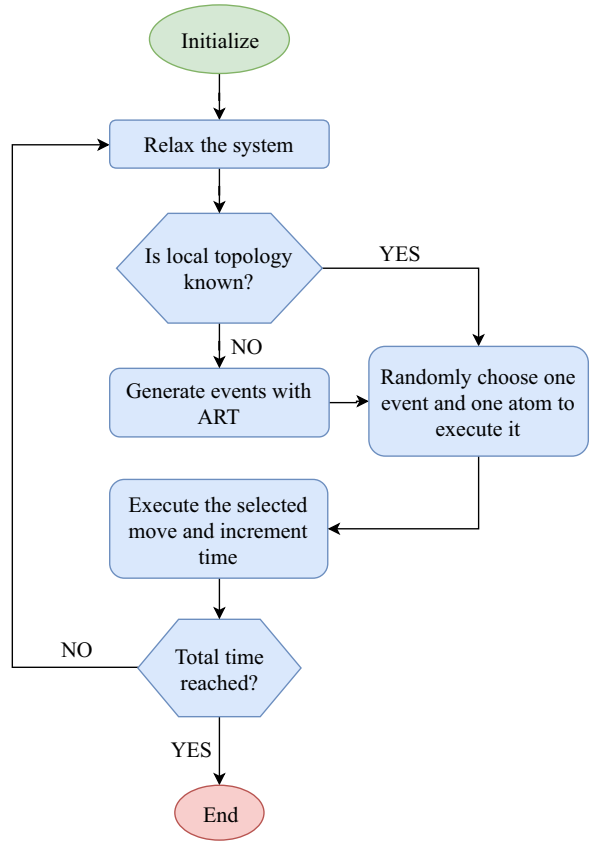

FIG. 1. Flowchart of the k-ART structure.

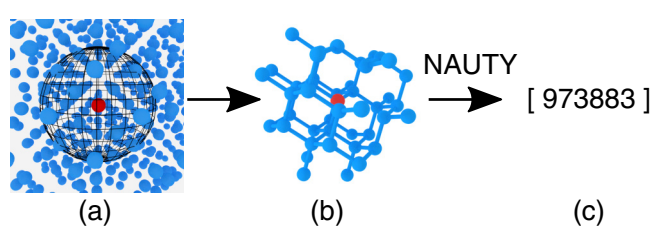

FIG. 2. Schematic illustration of the topological classification procedure where the red atom is in the center of the local graph. (a) is the initial configuration with the topology sphere, and (b) is the cluster of atoms within the sphere. A connectivity graph is extracted and analyzed by NAUTY, which returns (c) a unique label characteristic of the graph's topology.

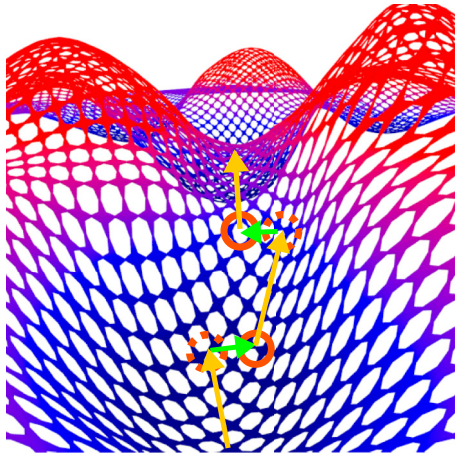

FIG. 3. Illustration of a complex energy landscape. The searches for saddle require random displacements followed by relaxation of the orthogonal forces in the hyperplane until the first-order saddle point is reached. The dashed circles represents the configuration on the energy surface before relaxation and the solid circles represent configuration after relaxation.

that takes into account short- and long-range interactions, including elastic deformations.

2. Saddle point search: ART nouveau

Open-ended search algorithms for saddle points make it possible to explore all transitions surrounding a local minimum in complex structures, schematically illustrated in Fig. 3. K-ART uses the ART nouveau [32,33] algorithm to search for saddle points that included a Lanczos-based approach for efficiently finding the lowest eigenvalues and corresponding eigenvectors of the Hessian matrix.

Several independent searches for saddle points are launched from each unique topology in the system following a three-step procedure: random displacements, following the path of negative curvature, and relaxation into a new minimum.

The initial displacement is introduced by pushing a given atom, or a set of atoms, in an arbitrary direction. The system is considered to be out of the harmonic well when the lowest eigenvalue of the Hessian matrix, computed using the Lanczos algorithm, becomes negative. Once outside the harmonic well, the system is pushed along the direction of negative curvature represented by the dashed circles in Fig. 3. Forces are minimized in the hyperplane orthogonal to this direction after each push (solid circles). This step is repeated until the total force becomes less than a preset threshold, indicating that a first-order saddle point is reached. The configuration is then pushed over the saddle point and relaxed into a new energy minimum.

The initial, saddle and final configurations are identified by means of topology, thus providing a unique label for each event that is used to create a catalog of possible events in the system. It is assumed that all atoms that share the same topology will have access to the same set of events, called *generic events*. To ensure a complete catalog of events, searches for events are not limited to new topologies; additional searches are launched proportional to the logarithm of the frequency for which a topology is encountered during the simulation.

3. Analysis and selection of the events

Once the catalog of events is up-to-date, all events are analyzed. The associated rates r_i of the events i is given as

$$r_i = \Gamma_0 \exp\left(-\frac{\Delta E}{k_B T}\right), \tag{1}$$

where $\Delta E = E_{\text{saddle}} - E_{\text{initial}}$ is the energy barrier; k_B is the Boltzmann's constant; T is the temperature; Γ_0 is a prefactor described by the transmission coefficient and the attempt frequency, which is fixed to 10^{13} s^{-1} at the onset of the simulation [30].

All generic events are ordered according to their energy barrier. The lowest-energy barrier events that make up to 99.9% of the total rate are fully reconstructed and their structure relaxed to a local energy minimum or converged to the saddle point, resulting in what we call *specific events*. The remaining events, that contribute very little to the rate, are cloned which means that the events are not fully reconstructed and the short- and long-range elastic interactions for these unlikely events are not fully accounted for. At this point, an event is chosen following the standard KMC algorithm. The elapsed time t is computed as

$$t = -\frac{\ln \mu}{r_i}, \tag{2}$$

where μ is a random number and r_i is the rate of the associated events. If the total time is reached the code stops, otherwise it goes back to the topology analysis step as seen in Fig. 1.

To sum up, k-ART makes use of a unique topology classification coupled with an unbiased, open-ended search for saddle points, while considering short- and long-range interactions due to elastic effects. An extensive catalog of the events are created on-the-fly which speeds up the simulation as the system evolves. In the past, k-ART has been used in various systems to describe diffusion of point defects in metals and semiconductors [34–36] and more complex systems with grain boundaries and amorphous silicon [37,38].

There exists another off-lattice KMC code, based on the dimer method, the self-evolving atomistic KMC (SEAKMC) [39,40] which has been found to show comparable performances to k-ART [41]. We selected k-ART because of its topological classification, that provides more flexibility to classify disordered systems, although the implementation of activation volume in SEAKMC gives a speed-up in performance in near-crystalline environments.

B. Model

The simulated system contains a kinked screw dislocation in the diamond lattice structure. The kink is created by stacking two substructures containing a 10b long screw dislocation which is shifted one Burgers vector in respect to the other, where b represents the length of the Burgers vector. The initial atomic positions for each substructure are created by calculating the displacement field based on elastic theory for screw dislocations [5]. The left and right dislocation

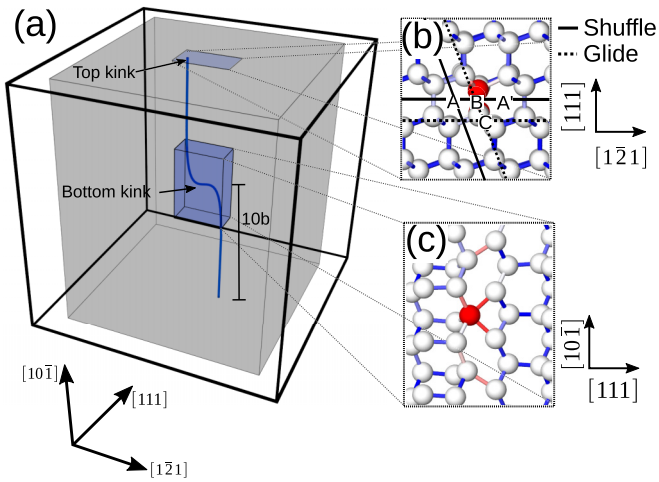

FIG. 4. (a) Schematic illustration of simulation box with two dislocation segments of length 10b. The atoms are represented by the gray area, which is surrounded by a vacuum layer of 10 Å along x and y surfaces. Dislocation segment 1 lies in position A, while segment 2 lies in position A', resulting in a kink positioned in position B (mixed shuffle/glide set). The periodic boundary condition along z direction results in a kink pair (top and bottom kink). In (b), the atomic structure projected along [10$\bar{1}$] is shown, while (c) shows the atomic structure in the bottom kink projected along [1$\bar{2}$1]. The red atom represents an overcoordinated atom, connecting the two opposing dimers.

segments are placed in the shuffle set denoted A and A', respectively. The two segments are displaced 1b along the slip direction, resulting in two dimers tilted in opposite directions relative to the [$\bar{1}$01] direction, as illustrated in Fig. 4(a). Each kink consists of a 5-coordinated atom positioned at B, which corresponds to the mixed shuffle/glide set. The overcoordinated atom connects the opposing dimers, thus connecting the dislocations segments lying in the A and A' positions.

The simulation box has dimensions 152 × 151 × 77 Å and contains 67 200 atoms. It is oriented such that the x, y, and z axes correspond to [1$\bar{2}$1], [111], and [10$\bar{1}$], respectively. The lattice parameter a_0 is set to 5.430 Å based on the experimental value found at 300 K [42]. Vacuum is added on the surfaces with the x and y axes as normal. The surface normal to the x axis is free to relax to minimize surface effects. However, the surface normal to the y axis is rigidly shifted and held fixed to maintain the stress field due to shearing. The simulation cell is sufficiently large so that any surface effects on the core structure and the dislocation motion is negligible. Periodic boundary conditions is applied along [10$\bar{1}$], which means the system is an infinite kinked screw dislocation with 10b separation between the kinks, which is sufficiently large that any kink-kink interactions can be neglected.

C. Simulation details

Atomic interactions are modeled using the environmental-dependent interatomic potential (EDIP) [43,44] as implemented in the Large-scale Atomic/Molecular Massively Parallel Simulator (LAMMPS) [45]. LAMMPS is coupled to k-ART as a library and is used as a force calculator. K-ART is used to explore the energy pathways and to simulate the evolution of the system. A sphere containing 47 ± 2 atoms with a radius of 6.0 Å is used for the topological classification. The cluster size variation is due to local distortions. During the search for saddle points, the total forces ($\sqrt{\sum_i^N \mathbf{F}_i^2}$) are relaxed with a convergence criterion of 0.05 eV/Å, while each minimum is relaxed to a convergence of 0.0005 eV/Å. Events with energy barriers higher than 2.7 eV are ignored, which corresponds to events with very low rates occurring on timescales out of interest. For all newly encountered topologies, the search for new saddle points is launched 10 times. The atomic structures are visualized in Open Visualization Tool (OVITO) [46].

Because of the covalent nature and high activation energy for dislocation movement in silicon, slip is expected to occur at elevated temperatures, or with high external stresses. It is well known that the activity of dislocations in silicon decreases substantially when reducing the temperature. This work is related to investigation of dislocation evolution during solidification; therefore, the temperature is set to 900 K for all simulations when calculating the transition rate. Furthermore, 900 K is already low compared to the melting temperature of silicon, which is as high as 1690 K.

In mc-Si, atoms are subjected to external stresses which affects the dislocation motion. Sources of stress can be grain boundary interfaces and thermal stresses generated during heating and cooling. External stress can affect the energy barriers and mechanisms for dislocation motion, and to investigate the effect of shear stresses, the model is subjected to a shear stress before the onset of the simulation. The shear stress is applied on the surface parallel to the {111} planes, which promotes motion of screw dislocations along [1$\bar{2}$1]. After the application of the shear stress, the forces are minimized with a convergence criterion of 0.0005 eV/Å. To ensure a constant shear stress, application of shear stress is repeated after each KMC step together with a relaxation of the forces to ensure the configuration is still kept in an energy minimum.

III. RESULTS AND DISCUSSION

A. Time evolution

Utilizing a KMC scheme gives us the possibility to explore mechanisms at timescales unattainable for conventional molecular dynamics. In Fig. 5, the time evolution (left axis) and the cumulative topologies (right axis) for kink migration and kink-pair formation is presented for all three stress levels. The kinetics is divided in three regions: kink migration (green), kink-pair formation (yellow), and creation of defects along the dislocation line without creating a stable kink (gray).

Kink migration at 900 K occurs on the femtosecond scale, and the plateaus in time evolution for 0.0 and 0.5 GPa, indicates that kink migration does not significantly contribute to the time evolution. However, with 1.0-GPa applied shear stress, kink migration, formation and the creation of defects occurs on the same timescale of femtoseconds. The major contribution to the time at 0.0 and 0.5-GPa shear stress is the creation of defects along the straight dislocation, where these events are at the nanoscale. However, oscillations between various defects can occur if the simulation does not find a stable kink configuration, which indeed happened in the nonstress simulation.

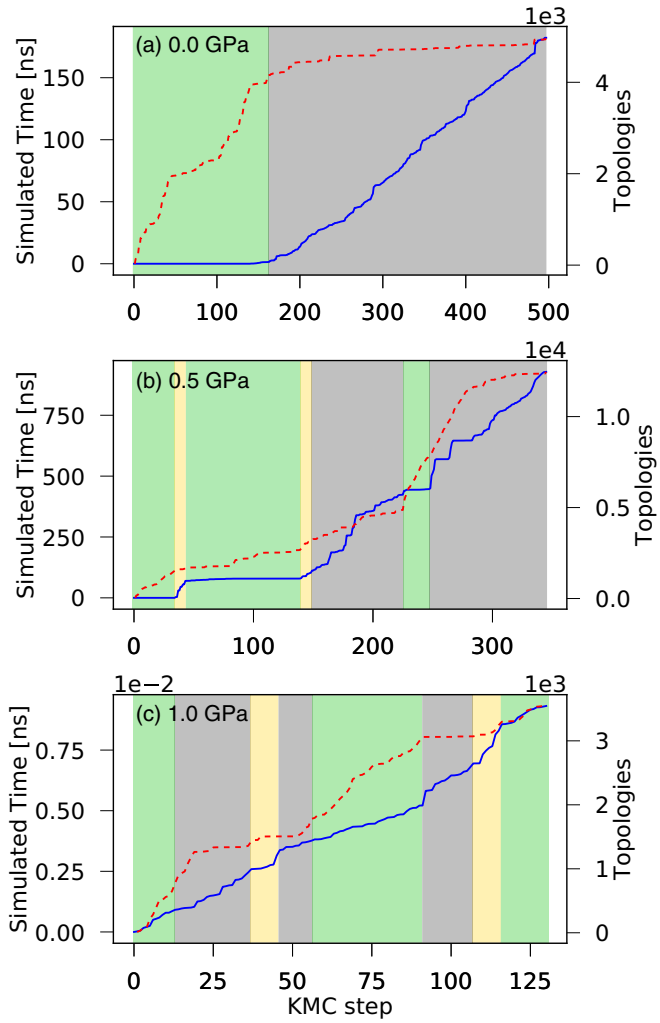

FIG. 5. Simulated time (solid line) and cumulative topologies (dashed line) as a function of KMC step for (a) 0.0, (b) 0.5, and (c) 1.0 GPa.

Cumulative topologies (dashed lines) for all stress levels are shown in Fig. 5. For shear stress of 0.0, 0.5, and 1.0 GPa, k-ART identifies 4974, 12 458, and 3545 topologies in total, respectively. Among these topologies, the number of unique topologies visited for the respective stress levels are 242, 367, and 176. The majority of the events are either unstable kinks during migration and formation of other point defects along the dislocation line.

There are two main features of the cumulative topology plot, which can be described as exploration of new topologies or oscillations between already encountered topologies. The exploration of new topologies is illustrated by the increase in cumulative topologies, where the simulation visits unexplored configurations. Plateaus on the topology curve indicates recycling of topologies already encountered.

B. Kink migration

1. Atomic structure

Kink migration from the initial kinked screw dislocation described in Sec. II B is first studied. The initial kink contains one 5-coordinated atom in position *B*, which is considered to be the ground state. K-ART identified four different mechanisms leading to kink migration, denoted mechanism M_1^m, M_2^m, M_3^m, and M_4^m. Several stable configurations that participate in the kink migration are observed, illustrated in Fig. 6. Mechanism M_1^m (solid lines) visits one intermediate configuration, M_2^m (dashed-dotted lines) is a direct transition, while M_3^m (dashed lines) and M_4^m (long-dashed lines) visit three intermediate configurations. Their associated forward energy barriers for each intermediate step during the kink migration are marked along their corresponding pathway. The intermediate kink structures, which can be described as one, three or five 5-coordinated atoms within the kink, are marked as the red atoms in Fig. 6. For simplicity, we denote these overcoordinated kink structures as (*m*,*n*) kinks, where *m* is the number of atoms that are *n*-coordinated, e.g., (1,5) kink represents the configuration with one 5-coordinated atom in the kink.

The bond length is sketched with the color gradient (blue, white, red) in Fig. 6. The bonds associated with the overcoordianted atom(s) are characterized by a length of 2.53 Å which is stretched compared to bulk length of 2.35 Å. For the (3,5) and (5,5) kinks, the bond lengths between the overcoordinated chain of atoms is in the range of 2.53 and 2.57 Å, where the higher end of the range is observed in the middle of the chain. The atoms exhibiting these stretched bonds are the most active during kink migration.

All four kink migration mechanisms can be described as a sequence of bond breaking and creation. Mechanism M_1^m is initiated by movement of atoms 3 and 9 toward each other to create a bond resulting in three overcoordinated atoms. This results in the intermediate (3,5)-kink configuration. To complete the kink migration, atoms 1 and 9 move in opposite directions, breaking the bond between them and resulting in the (1,5) kink, which has migrated a distance of 1b along [101]. M_3^m is similar to M_1^m, where the first intermediate kink structure is the (3,5)-kink structure and second intermediate step results in the (5,5)-kink structure by movement of atoms 5 and 7 toward each other. Two subsequent events occur with a similar mechanism as M_1^m where a single bond is broken due to two atoms moving apart from each other. M_2^m is a direct transition where the bond between atoms 1 and 9 is broken simultaneously that a bond between atoms 3 and 9 is created. Mechanism M_4^m is initiated by movement of atoms 2 and 9 move towards each other, resulting in overcoordination of atoms 1, 2, and 9. This kink is termed the $(3,5)'$ kink. The next event consists of repulsion between atoms 1 and 9 resulting in overcoordination on atom 3, named the $(1,5)'$ kink. The next event consists of an attraction of atoms 3 and 9, forming a quasisymmetrical $(3,5)'$ kink. The structure appears to be symmetrical, but due to local variation of the strain, the energy pathway is asymmetrical, which is shown in the next section in Fig. 7. To complete the kink migration, atoms 2 and 9 move apart from each other resulting in the a new (1,5) kink, which have migrated a distance of 1b along [101].

The (1,5) kink is considered to be the ground state, where the (3,5) kink has an energy that is 0.09 eV higher compared to the ground state, which is similar to the reported value based on NEB simulations with EDIP [22]. However, two new kink structures emerge here: the $(3,5)'$ kink, which has a core

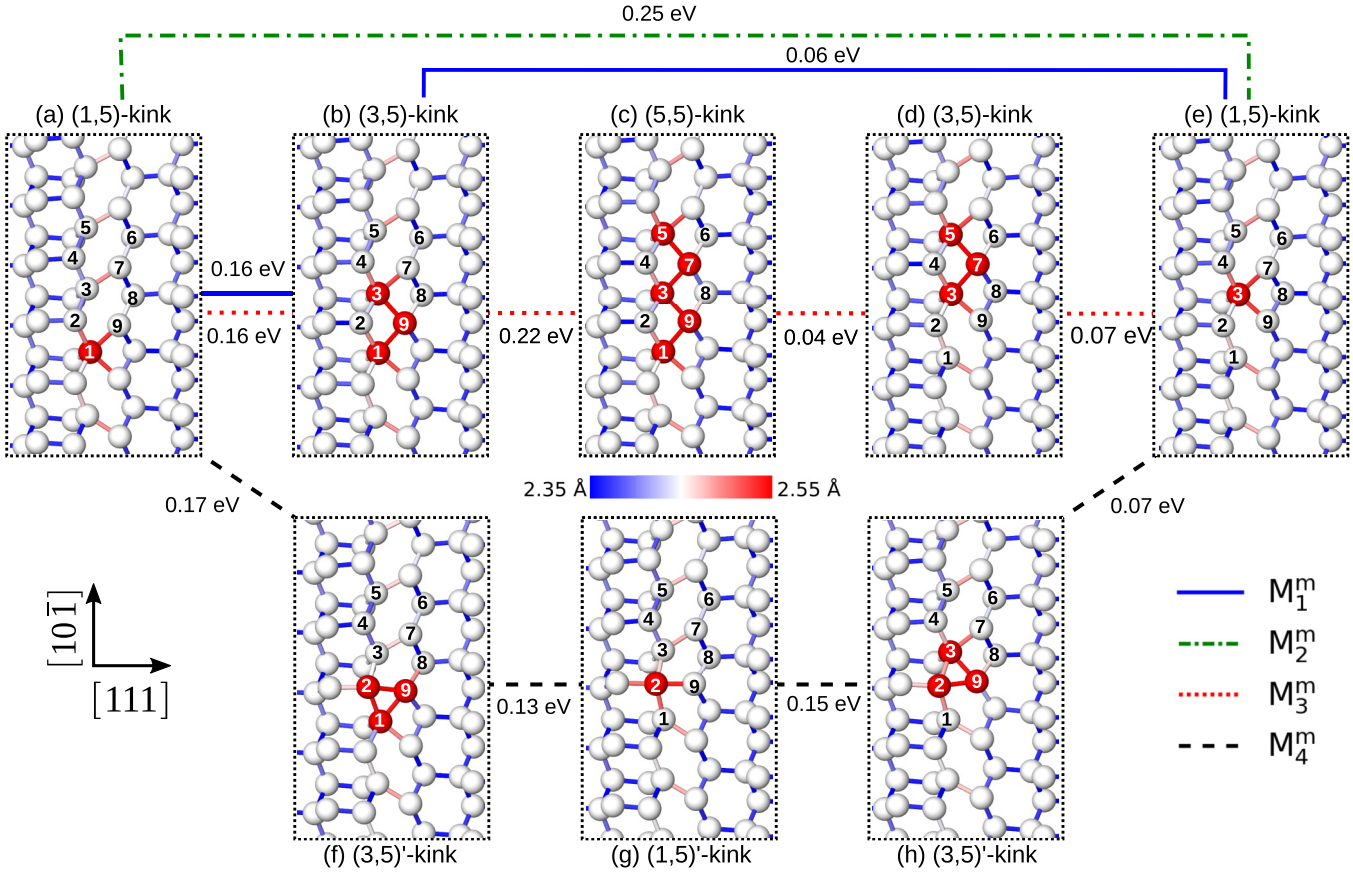

FIG. 6. Atomistic representation of stable kink structures projected along [1$\bar{2}$1]. The solid, dashed-dot, and dashed lines correspond to mechanism M_1^m, M_2^m, and M_3^m, respectively. The color bar represents the bond length, and red atoms are overcoordinated atoms.

energy of 0.08 eV above the ground state; the $(1,5)'$ kink, which has a core energy of 0.10 eV above the ground state. Because the energy differences between the stable kink structures are very small, there would be an oscillation between the kink structures at finite temperature. The (1,5)-kink and (3,5)-kink structures have been described by Pizzagalli *et al.* [22] as narrow and wide kinks, respectively; while the authors also observed a kink structure with a dangling bond with DFT calculations. The core energy was degenerated according to their DFT calculations. Due to the size restriction with DFT, no conclusions was made based on which core is the most stable. However, since the energy difference is small, the kink should not be confined to a single geometry for a very long time [22].

In our study, a (5,5) kink is observed to participate in kink migration acting as an intermediate configuration, which has not been previously described. The core energy of the (5,5) kink has an energy 0.28 eV higher than the ground state. Interestingly, a (7,5) kink is also observed during the simulation, however, this kink does not participate in kink migration but acts as a metastable structure with an energy of 0.4 eV higher than the ground state. In fact, these wide kinks can be described as dislocation segments in position *B*. Calculations based on the EDIP and Tersoff potentials [47],

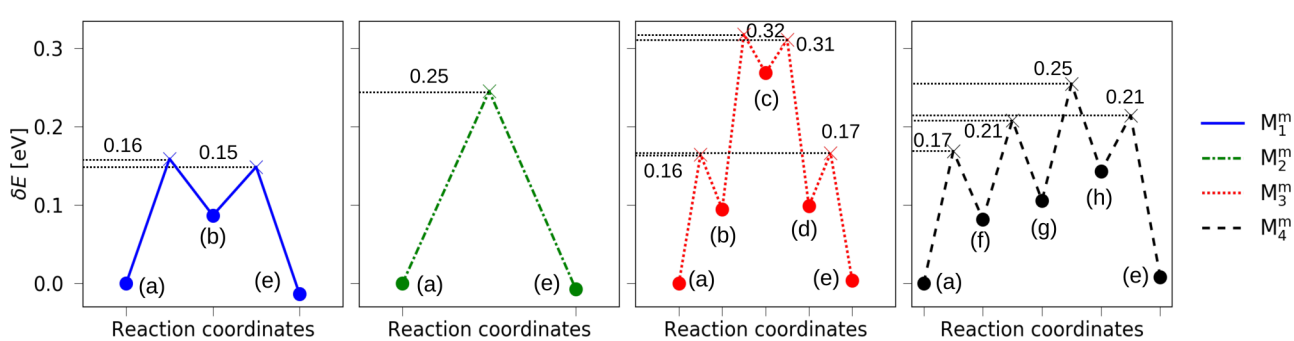

FIG. 7. The minimum energy pathway for the different mechanisms is shown, where the circles and crosses represent minimum and saddle points, respectively. The saddle point energy relative to the ground state is indicated by the dashed horizontal line. The labels correspond to their respective kink configuration as shown in Fig. 6. The lines act as a guide for the eye.

TABLE I. Comparison of the total activation energy for kink migration found in this study. Three methods are considered: K-ART, dimer method and NEB. The force calculations of the different simulations are based on various interatomic potentials (EDIP, Tersoff and Lenosky) and DFT.

	Method	Potential	Activation energy (eV)
This work	K-ART	EDIP	0.16[a]
			0.25
			0.32[b]
			0.25[b]
Pedersen *et al.* [23]	Dimer	Lenosky	0.07
	Dimer	EDIP	0.17[a]
			0.25
			0.33[a]
	Dimer	Tersoff	0.18[a]
Pizzagalli *et al.* [22]	NEB	DFT	0.075
	NEB	EDIP	0.158[a]

[a]One intermediate configuration.
[b]Three intermediate configurations.

show that straight dislocations lying in position B are unstable. Nevertheless, there is a study suggesting that dislocations in position B could act as intermediate steps in core transformations from shuffle to glide character and dissociation of the glide dislocation [48]; however, this transition pathway would be more complicated in comparison to a direct transition from shuffle to glide [49].

2. *Energy pathways*

The energy pathways for the kink migration mechanisms are shown in Fig. 7, with the same line style as the top panel. The first step of mechanism, M_1^m, has an energy barrier of 0.15 eV followed up with an transition of 0.06 eV to complete the kink migration. Mechanism M_2^m is a direct kink migration which includes crossing of a single barrier of 0.25 eV. Mechanism M_3^m is the mechanism which follows the highest energy pathway, with two initial steps with energy barriers of 0.16 and 0.22 eV. The two subsequent events completes the kink migration with energy barriers of 0.05 and 0.07 eV. The first three events of mechanism M_4^m have energy barriers of 0,17, 0.13, and 0.15 eV, and the event that completes the kink migration has a barrier of 0.07 eV. Figure 7 shows an asymmetrical minimum energy pathway for mechanism M_4^m. Among these four kink migration mechanisms, M_1^m is the mechanism that exhibits the lowest maximal energy barrier, which makes mechanism M_1^m the most probable. However, mechanism M_4^m exhibit similar barriers compared to M_1^m, thus is also considered to be a highly probable mechanism for kink migration.

The total activation energy is considered to be the maximum increase of energy along the energy pathway in comparison to the ground state. For the mechanism M_1^m, M_2^m, M_3^m, and M_4^m, the activation energy is calculated to be 0.16, 0.25, 0.32, and 0.25 eV, respectively. A comparison between the values calculated by the present simulations and the results by Pizzagalli *et al.* [22] and Pedersen *et al.* [23] are summarized in Table I. An excellent compliance between the various methods based on the EDIP (NEB and dimer method) and Tersoff potential (dimer method) is observed. However, simulations based on DFT calculations with NEB method and based on the Lenosky potential together with the dimer method show lower kink migration barriers in comparison with the other potentials. Simulations based on DFT calculations and the Lenosky potential are reported to prefer undercoordination of the atoms in the kink structure, leading to a dangling bond in the kink; whilst, the EDIP and Tersoff potentials prefer overcoordination [23].

Despite the discrepancies in atomic structure with the different potentials, the mechanisms for kink migration are comparable; that is, kink migration consists of a sequence of breaking and creation of bonds for all potentials and methods.

3. *Effect of thermal expansion*

Simulations based on KMC usually neglect temperature effects like thermal expansion on the energy barriers. The impact of omitting the thermal expansion has been investigated by running additional k-ART simulations with initial structures based on experimental lattice parameters at 900 K ($a_0 = 5.437$ Å) and 1500 K ($a_0 = 5.457$ Å) [42]. Showing a difference of less than 0.01 eV, the energy barrier for kink migration is only weakly influenced by thermal expansion. Noteworthy, the deviation cannot only be correlated to thermal expansion. Local deformations and elastic interactions, due to the kink-kink or kink-surface separation are not necessarily equal in all instances, can contribute to the small deviation. However, the atomistic details of the migration mechanisms are left unchanged. Furthermore, an increase in temperature gives higher entropic contribution to the free energy, affecting the dislocation motion; however, this effect is not investigated in this study.

4. *Effect of shear stress*

The effect of shear stress on energy barriers related to kink migration is illustrated in Fig. 8, which shows the cumulative distribution of available events during kink migration. Events with an energy barrier above 0.6 eV are omitted, since these barriers are never selected during kink migration. Energy barriers for each mechanism are marked with the black arrows. For mechanism M_3^m and M_4^m, which have several barriers of similar value, the arrow indicates the energy region where these events occur. In the nonstressed condition, all events associated with mechanism M_1^m, M_3^m, and M_4^m exhibit energy barriers lower than the energy barrier for mechanisms M_2^m, where the latter is the least probable mechanism, as discussed in Sec. III B. Interestingly, the shear stress decreases the energy barrier for the event associated with mechanism M_2^m, while the energy barriers for mechanism M_1^m, M_3^m and M_4^m remains the same or increases. For shear stresses of 0.5 and 1.0 GPa, the energy barrier for mechanism M_2^m is calculated to be 0.16 and 0.13 eV, respectively; therefore, M_2^m becomes the dominating mechanism for kink migration. Noteworthy, with the application of shear stress, the energy pathway for mechanism M_1^m was explored only once, while the higher energy pathways for mechanism M_3^m and M_4^m were left unexplored.

To explain the shift in energy barriers, we look at the atomic bonds in the kink. The shear stress slightly change

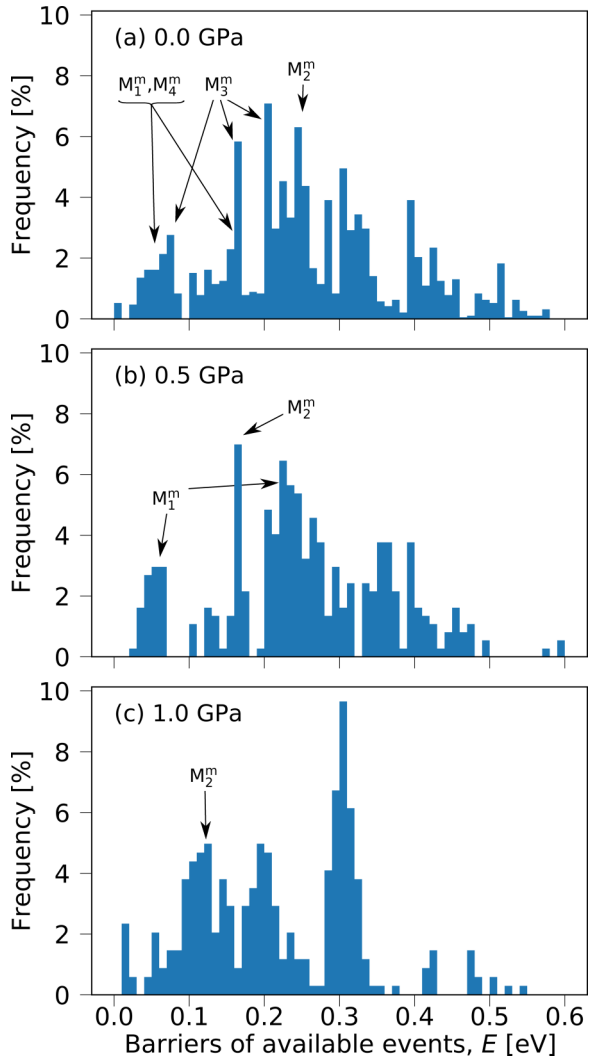

FIG. 8. Cumulative distribution of the energy barriers of the available events during kink migration. The associated energy barriers for kink migration is marked with the black arrows. A shift in energy barriers for mechanism M_2^m is observed with application of shear stress, changing the preferred mechanism for kink migration to mechanism M_2^m.

the bond lengths between the atoms directly connected to the overcoordinated atom. In the top kink, the bond above the overcoordinated atom is slightly reduced in length from 2.53 Å in the nonstressed condition to 2.52 and 2.50 Å with shear stresses of 0.5 and 1.0 GPa, respectively. Below the top-kink, the bond is slightly extended from 2.53 Å for the nonstressed condition, to 2.54 and 2.56 Å for shear stress of 0.5 and 1.0 GPa, respectively. The opposite effect is observed for the bottom kink. As described in Sec. III B 1, kink migration is described as creating and breaking bonds; the extended bonds would require less energy to break resulting in greater attraction between the kink pairs, and a higher diffusion rate for kink migration.

C. Kink-pair formation

After a kink has successfully migrated and annihilated, a 20b long straight dislocation is created. From a straight

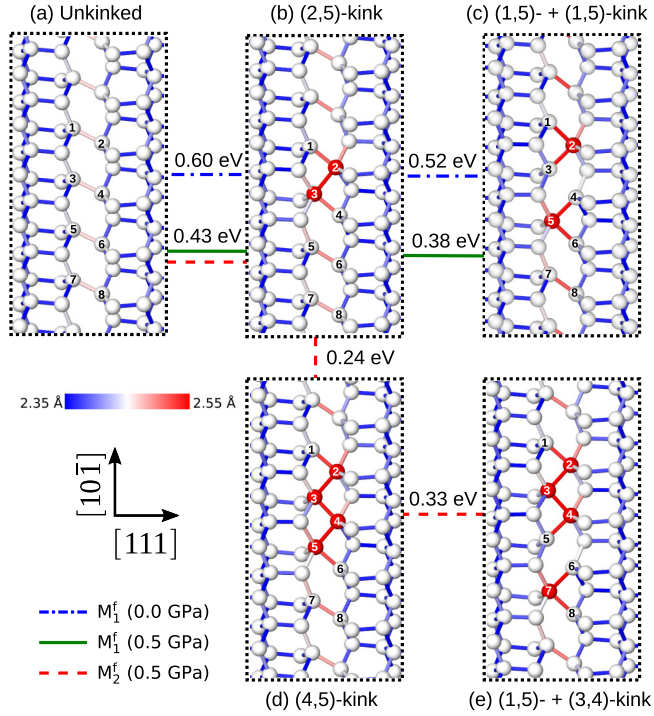

FIG. 9. Two mechanisms are encountered, M_1^f (solid and dashed-dotted lines) and M_2^f (dashed line), the former is observed in the nonstressed and stressed conditions, while the latter is observed only with 0.5-GPa shear stress. The ball-stick models illustrates the atomic configurations with same color scheme as Fig. 4. The numbers indicates the atoms that participate in kink-pair formation. The forward barriers for each mechanism is indicated between the configurations.

kink-free dislocation, the kink-pair formation is studied within the same simulations with an applied shear stress of 0.0 and 0.5 GPa, respectively.

In the nonstressed simulation, no stable kink pair is created due to the asymmetric energy landscape, that is, a very high forward barrier and very low backward barrier. The reversed energy pathway for kink-pair formation, i.e., annihilation of kink pairs is reported instead. K-ART imposes detailed balance when finding events, i.e., all reverse events are automatically added to the catalog. Therefore the atomic details of kink-pair formation in the nonstressed condition are still valid.

For the simulation with 1.0 GPa, several point defects are generated along the dislocation line resulting in a very distorted dislocation line. Due to the distortions, derivation of a minimum energy pathway with well-defined kink structures was not possible, and is thus not included in the following sections.

1. Atomic structure

The atomic details of each mechanism with a shear stress of 0.0 and 0.5 GPa are illustrated in Fig. 9. A single mechanism, M_1^f, leading to stable kink pairs, is observed for both stress levels, resulting in the formation of a pair of (1,5) kinks. A second mechanism, M_2^f, is explored in the simulation with a shear stress of 0.5 GPa, resulting in a pair of a (1,5) kink and

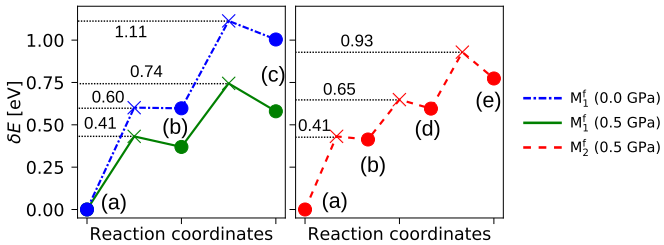

FIG. 10. Minimum energy pathway for kink-pair formation with shear stress of 0.0 and 0.5 GPa. Two mechanisms are observed, named M_1^f and M_2^f, where the latter is only observed for the 0.5 GPa simulation. The labels correspond to their respective kink configuration as shown in Fig. 9. The lines act as a guide for the eye.

a (3,5) kink. A stable kink pair is fully developed when the opposing tilt direction of the stacked {111} plane is observed in between the overcoordinated atoms, as shown in Figs. 9(c) and 9(e).

The initial step in the kink-pair formation for both M_1^f and M_2^f is initiated by movement of atoms 2 and 3 toward each other, creating a bond between the two atoms. The result is a (2,5) half-kink, which is an intermediate configuration where the dislocation has not fully slipped from one Peierls valley to a neighboring valley, resulting in a small dislocation segment lying in position *B*. A complete kink formation of the (1,5)-kink pair occurs by simultaneously breaking the bond between atoms 3 and 4, whilst creating a bond between atoms 4 and 5. Mechanism M_2^f exhibit similar kinetics as M_1^f. However, M_2^f includes a second intermediate configuration, which can be characterized as a (4,5) half-kink. Once created, the kink pairs can either annihilate each other or migrate further apart as described in Sec. III B.

2. *Energy pathways*

The energy pathways are shown in Fig. 10. The first step of mechanism M_1^f and M_2^f are interchangeable. With a shear stress of 0.0 and 0.5 GPa, the initial step has an energy barrier of 0.60 and 0.43 eV, respectively. The subsequent event to finish the kink-pair formation is calculated to have an energy barrier of 0.52 and 0.38 eV. For mechanism M_2^f, two subsequent events are required to complete the kink-pair formation, with barriers calculated to be 0.24 and 0.33 eV.

The mechanisms reported in this paper are mostly similar to the pathway described by Pizzagalli *et al.* [22] based on NEB and EDIP, where mechanism M_1^f starts and ends with the same configuration; however, the intermediate configurations are somewhat different. The pathway found by NEB with EDIP follows (a) → (b) → (d) → (c) in Fig. 10, whilst k-ART finds an energy pathway which follows the configurations (a) → (b) → (c). In our simulations, the kink-pair formation energy, i.e., the total activation energy, is calculated to be 1.11 and 0.74 eV for the systems subjected to 0.0 and 0.5 GPa of shear stress, respectively. In comparison, the authors of Ref. [22] reported a total activation energy of 0.91, 0.88, 0.83, and 0.79 eV for stress levels of 0.0, 0.31, 0.61, and 0.92 GPa, respectively. However, they used configuration (a) and (d) to calculate the kink-pair formation, which is an intermediate metastable half-kink and not a fully developed kink.

The energy pathway for mechanism M_2^f in our simulation visits configuration (d), i.e., the (4,5) half-kink. The activation energy with the (4,5) half-kink as the final configuration is 0.65 eV with 0.5 GPa applied shear stress, which is substantially lower than the estimated value of 0.83 eV with 0.61 GPa shear stress as reported in Ref. [22]. The boundary conditions used in this work and in the work in Ref. [22] are similar, and is based on the same interatomic potential; thus, the method is likely the reason for the difference.

The dimer calculations based on the Lenosky potential performed by Pedersen *et al.* [23] gives a total activation barrier of 1.19 eV, similar to the activation barrier found in this study of 1.11 eV. However, the dimer method as implemented in the study by Pedersen *et al.* [23] is not coupled to a KMC algorithm; therefore, the energy landscape from nonintuitive configurations could have been left unexplored, and pathways with lower activation energy containing such configurations could be missed.

In addition to the EDIP and NEB calculations, Pizzagalli *et al.* performed DFT calculations with NEB identified a total activation energy of 1.36 eV [22], which is higher than all calculated values based on other potentials independent of method. Because of the surface constraints, the authors concluded that the value obtained from DFT calculations serve as an upper limit, while their EDIP calculations serve as an lower limit. Thus the kink-pair formation should be in the range of 0.9 to 1.36 eV, which is in agreement with our work.

IV. SUMMARY

In this study we deploy a novel approach to simulate the mechanisms related to dislocation motion in silicon, that is, kink migration and kink-pair formation. Four mechanisms for kink migration are observed. The activation energies for the four mechanisms are calculated to be 0.16, 0.25, 0.32 and 0.25 eV, respectively. With the application of shear stress, the preferred mechanism for kink migration changes to mechanism M_2^m by lowering the energy barrier in comparison with the other mechanisms. Several new kink structures are explored, characterized as the $(1,5)'$, $(3,5)'$, (5,5), and (7,5) kinks; where the three former participates in kink migration. In particular, the $(1,5)'$ and $(3,5)'$ kinks are the part of a new kink migration mechanism. Two energy pathways for kink-pair formation are identified, resulting in a pair of two (1,5) kinks and a pair of (1,5) and (3,5) kinks. The former of the two mechanisms follows a pathway with a lower total activation energy than those previously described in the literature. The latter contains a higher energy pathway, and is only sampled at a shear stress of 0.5 GPa. At a temperature of 900 K, kink migration takes place on the femtosecond scale; whilst, kink-pair formation takes place after hundreds of nanoseconds.

To conclude, this study demonstrates that k-ART is a viable method to simulate the complex kinetics related to dislocation motion in silicon. A good agreement is found between the kink migration energies and kink-pair formation energies calculated with k-ART and the results obtained by

other methods, e.g., the NEB and dimer methods. In addition, new kink structures and unexplored energy pathways relevant for both kink migration and kink-pair formation are observed. With k-ART, the time step restriction associated with conventional molecular dynamics is relieved. Together with an unbiased search for saddle points, the complex energy landscape surrounding kink structures in silicon is thoroughly explored where new nontrivial and relevant structures have been presented.

These mechanisms are relevant for studying nucleation of dislocations from various dislocation sources, e.g., grain boundary junctions, k-ART can thus be used to fill in the missing information from nucleation of dislocation to characterization performed postmortem. Furthermore, k-ART has the potential to be applied to simulate the interactions between grain boundaries and dislocations. Future work in this direction can improve our understanding of the mechanisms behind dislocation generation in systems containing grain boundaries which can in turn help to increase material quality and the pursuit of a higher conversion efficiency in solar cells based on mc-Si.

The saddle point search algorithm ART nouveau is freely distributed [50]. K-ART and development ART nouveau are available upon request from Normand Mousseau.

ACKNOWLEDGMENTS

The authors gratefully acknowledge the high performance computing allocation from the NOTUR consortium (Projects No. nn9158k and No. nn9347k). This work is part of the INSIDES project (Project No. 255326) under the ENERGIX programme supported by the Research Council of Norway.

[1] *Fraunhofer Institute for Solar Energy Systems, Photovoltaics Report* (2017/2018).
[2] *International Technology Roadmap for Photovoltaic Results 2017*, 9th ed. (2018).
[3] A. D. Kurtz, S. A. Kulin, and B. L. Averbach, Phys. Rev. **101**, 1285 (1956).
[4] K. Adamczyk, R. Søndenå, C. C. You, G. Stokkan, J. Lindroos, M. Rinio, and M. Di Sabatino, Phys. Status Solidi (a) **215**, 1700493 (2017).
[5] J. P. Hirth and J. Lothe, *Theory of Dislocations*, 2th ed. (Krieger Publishing Company, Malabar, FL, 1992).
[6] H. Saka, K. Yamamoto, S. Arai, and K. Kuroda, Philos. Mag. **86**, 4841 (2006).
[7] H. R. Kolar, J. C. H. Spence, and H. Alexander, Phys. Rev. Lett. **77**, 4031 (1996).
[8] H. Alexander, J. c. H. Spence, D. Shindo, H. Gottschalk, and N. Long, Philos. Mag. A **53**, 627 (1986).
[9] T. Suzuki, T. Nishisako, T. Taru, and T. Yasutomi, Philos. Mag. Lett. **77**, 173 (1998).
[10] K. Asaoka, T. Umeda, S. Arai, and H. Saka, Mater. Sci. Eng. A **400-401**, 93 (2005).
[11] C.-Z. Wang, J. Li, K.-M. Ho, and S. Yip, Appl. Phys. Lett. **89**, 051910 (2006).
[12] L. Pizzagalli and P. Beauchamp, Philos. Mag. Lett. **88**, 421 (2008).
[13] M. S. Duesbery and G. Y. Richardson, Crit. Rev. Solid State Mater. Sci. **17**, 1 (1991).
[14] V. V. Bulatov, S. Yip, and A. S. Argon, Philos. Mag. A **72**, 453 (1995).
[15] V. V. Bulatov, J. F. Justo, W. Cai, S. Yip, A. S. Argon, T. Lenosky, M. de Koning, and T. D. de la Rubia, Philos. Mag. A **81**, 1257 (2001).
[16] W. Cai, V. V. Bulatov, and S. Yip, J. Comput,-Aided Mater. Des. **6**, 175 (1999).
[17] N. Oyama and T. Ohno, Phys. Rev. Lett. **93**, 195502 (2004).
[18] A. Valladares, J. A. White, and A. P. Sutton, Phys. Rev. Lett. **81**, 4903 (1998).
[19] S. Öberg, P. K. Sitch, R. Jones, and M. I. Heggie, Phys. Rev. B **51**, 13138 (1995).
[20] Y. M. Huang, J. C. H. Spence, and O. F. Sankey, Phys. Rev. Lett. **74**, 3392 (1995).
[21] R. W. Nunes, J. Bennetto, and D. Vanderbilt, Phys. Rev. B **58**, 12563 (1998).
[22] L. Pizzagalli, A. Pedersen, A. Arnaldsson, H. Jónsson, and P. Beauchamp, Phys. Rev. B **77**, 064106 (2008).
[23] A. Pedersen, L. Pizzagalli, and H. Jónsson, J. Phys.: Condens. Matter **21**, 084210 (2009).
[24] W. Cai, V. V. Bulatov, J. Chang, J. Li, and S. Yip, Dislocation core effects on mobility, in *Dislocations in Solids*, edited by F. R. N. Nabarro and J. P. Hirth, Vol. 12 (Elsevier, Amsterdam, 2004), Chap. 64, pp. 1–80.
[25] G. Henkelman, B. P. Uberuaga, and H. Jónsson, J. Chem. Phys. **113**, 9901 (2000).
[26] V. V. Bulatov, Scr. Mater. **45**, 1247 (2001).
[27] N. Mousseau, L. K. Béland, P. Brommer, F. El-Mellouhi, J.-F. Joly, G. K. N'Tsouaglo, O. Restrepo, and M. Trochet, Comput. Mater. Sci. **100**, 111 (2015), special Issue on Advanced Simulation Methods.
[28] M. Trochet, A. Sauvé-Lacoursière, and N. Mousseau, J. Chem. Phys. **147**, 152712 (2017).
[29] L. K. Béland, P. Brommer, F. El-Mellouhi, J. F. Joly, and N. Mousseau, Phys. Rev. E **84**, 046704 (2011).
[30] F. El-Mellouhi, N. Mousseau, and L. J. Lewis, Phys. Rev. B **78**, 153202 (2008).
[31] B. D. McKay and A. Piperno, J. Symbol. Comp. **60**, 94 (2014).
[32] G. T. Barkema and N. Mousseau, Phys. Rev. Lett. **77**, 4358 (1996).
[33] R. Malek and N. Mousseau, Phys. Rev. E **62**, 7723 (2000).
[34] S. Mahmoud, M. Trochet, O. A. Restrepo, and N. Mousseau, Acta Mater. **144**, 679 (2018).
[35] M. Trochet, L. K. Béland, J.-F. Joly, P. Brommer, and N. Mousseau, Phys. Rev. B **91**, 224106 (2015).
[36] M. Trochet and N. Mousseau, Phys. Rev. B **96**, 134118 (2017).
[37] O. A. Restrepo, N. Mousseau, M. Trochet, F. El-Mellouhi, O. Bouhali, and C. S. Becquart, Phys. Rev. B **97**, 054309 (2018).
[38] J.-F. Joly, L. K. Béland, P. Brommer, and N. Mousseau, Phys. Rev. B **87**, 144204 (2013).

[39] H. Xu, Y. N. Osetsky, and R. E. Stoller, Phys. Rev. B **84**, 132103 (2011).
[40] H. Xu, Y. N. Osetsky, and R. E. Stoller, J. Phys.: Condens. Matter **24**, 375402 (2012).
[41] L. K. Béland, Y. N. Osetsky, R. E. Stoller, and H. Xu, Comput. Mater. Sci. **100**, 124 (2015), special Issue on Advanced Simulation Methods.
[42] Y. Okada and Y. Tokumaru, J. Appl. Phys. **56**, 314 (1984).
[43] M. Z. Bazant, E. Kaxiras, and J. F. Justo, Phys. Rev. B **56**, 8542 (1997).
[44] J. F. Justo, M. Z. Bazant, E. Kaxiras, V. V. Bulatov, and S. Yip, Phys. Rev. B **58**, 2539 (1998).
[45] S. Plimpton, J. Comput. Phys. **117**, 1 (1995).
[46] A. Stukowski, Modell. Simul. Mater. Sci. Eng. **18**, 015012 (2009).
[47] L. Pizzagalli, P. Beauchamp, and J. Rabier, Philos. Mag. **83**, 1191 (2003).
[48] L. Pizzagalli, J. Mater. Sci. **51**, 2869 (2016).
[49] J. Guénolé, J. Godet, and L. Pizzagalli, Modell. Simul. Mater. Sci. Eng. **18**, 065001 (2010).
[50] www.normandmousseau.com.